Studii şi Cercetări Ştiinţifice 2014, **15** (3), pp. 197 – 212
Chimie şi Inginerie Chimică, Biotehnologii, Industrie Alimentară

Scientific Study & Research
Chemistry & Chemical Engineering, Biotechnology, Food Industry *ISSN 1582-540X*

ORIGINAL RESEARCH PAPER

CATALYTIC COMBUSTION OF METHANE OVER Pt/γ-Al_2O_3 IN MICRO-COMBUSTOR WITH DETAILED CHEMICAL KINETIC MECHANISMS

Junjie Chen*, Xuhui Gao

Henan Polytechnic University, School of Mechanical and Power Engineering, 454000, Jiaozuo, China

*Corresponding author: comcjj@163.com

Received: July 16, 2014
Accepted: September 30, 2014

Abstract: Micro-scale catalytic combustion characteristics and heat transfer processes of preheated methane-air mixtures (φ = 0.4) in the plane channel were investigated numerically with detailed chemical kinetic mechanisms. The plane channel of length L = 10.0 mm, height H =1.0 mm and wall thickness δ = 0.1 mm, which inner horizontal surfaces contained Pt/γ-Al_2O_3 catalyst washcoat. The computational results indicate that the presence of the gas phase reactions extends mildly the micro-combustion stability limits at low and moderate inlet velocities due to the strong flames establishment, and have a more profound effect on extending the high-velocity blowout limits by allowing for additional heat release originating mainly from the incomplete CH_4 gas phase oxidation in the plane channel. When the same mass flow rate ($\rho_{in} \times V_{in}$) is considered, the micro-combustion stability limits at p: 0.1 MPa are much narrower than at p: 0.6 MPa due to both gas phase and catalytic reaction activities decline with decreasing pressure. Catalytic micro-combustor can achieve stable combustion at low solid thermal conductivity k_s < 0.1 $W \cdot m^{-1} \cdot K^{-1}$, while the micro-combustion extinction limits reach their larger extent for the higher thermal conductivity k_s = 20.0-100.0 $W \cdot m^{-1} \cdot K^{-1}$. The existence of surface radiation heat transfers significantly effects on the micro-combustion stability limits and micro-combustors energy balance. Finally, gas phase combustion in catalytic micro-combustors can be sustained at the sub-millimeter scale (plane channel height of 0.25 mm).

Keywords: *catalytic combustion, chemical kinetic mechanisms, micro-combustion, stability limits, combustion characteristics, heat transfer*

INTRODUCTION

The high energy density of hydrocarbon fuels (such as propane, methane, and octane, etc.) creates a great opportunity to develop combustion based micro-scale power generation systems to meet increasing demands for portable power devices, micro-satellite thrusters, micro chemical reactors, micro unmanned aerial vehicles, and micro sensors [1]. The gas phase combustion of methane-air mixtures can be sustained at the sub-millimeter scale in micro-combustors with appropriately annealed walls that mitigate radical quenching [2]. Moreover, practical configurations such as the heat-recirculating and excess enthalpy ("Swiss-roll") micro-combustors have been shown to stabilize the flames of propane/air mixtures for small channel widths of 3.5 mm [3]. Despite the feasibility of micro-scale gaseous combustors, the associated large S/V (surface-to-volume) ratios at the micro-scale give rise to flame stabilization difficulties due to thermal and radical quenching on the micro-combustor walls [4]. Catalytic combustion is a plausible solution to overcome these issues [5], since it complies with the requirements of large S/V ratios and moderate combustion temperatures relevant to micro-scale power generation devices. The noble metal catalysts (such as Pt, Pd, Rh, etc.) are employed in most cases, due to their lower activation energy for the total oxidation and reforming of hydrocarbon fuels at modest reactor temperatures [6]. More recent experimental works have therefore focused on hydrocarbon and hydrogen catalytic combustion in a variety of micro-combustors configurations [4-10]. The preferred catalyst in those studies was the noble metal catalysts Pt.

In order to improve combustion stability and thermal efficiency of micro combustors, various efforts have been paid to the optimization of thermal management, design and the use of catalyst. The stability of gas phase combustion of methane-air, propane-air, and propylene-air mixtures has been investigated numerically and experimentally [11, 12] in channels with sub-millimeter gap sizes and walls without radical quenching. Therein, numerical simulations with a one-step gaseous reaction were utilized to elucidate the effect of heat transfer mechanisms on the energy management of micro-combustors. Combustion stability issues were investigated in a 2.2-mm-gap channel with 2-D CFD simulations [13] in the catalytic micro-combustors of methane-air mixtures over catalysts Pt; the detailed catalytic reaction mechanism was used [14] and the thermally thin wall assumption was invoked. The extinction limits have been mapped out experimentally for non-catalytic and catalytic combustion of propane/air mixtures in the heat recirculating "Swiss-roll" micro-combustors [15].

The contribution of gas phase reactions cannot continue to be ignored in catalytic micro-combustors, despite the large S/V ratios of micro-combustors. Typically, micro-combustors employ very low inlet velocities (e.g. less than 0.5 $m \cdot s^{-1}$), which lead to sufficiently long residence times for the heat up and gas phase ignition in the micro-chamber. Validated gas phase and catalytic chemical kinetics are indispensable inputs in the design of catalytic micro-combustors. The importance of suitable catalytic and gas phase chemical kinetics should not be understated in micro-combustor studies. For instance, the onset of gas phase ignition requires the gas phase chemical reaction schemes that can accurately catch the ignition delay characteristics in the presence of the catalytic pathway. The flame anchoring position impacts the associated extinction limits and the heat transfer mechanisms in turn. The advancement of catalytic combustion in micro-scale power systems requires the development of catalysts with

increased activity toward the complete oxidation of methane in the micro-chamber, the understanding of the low-temperature gas phase and the catalytic chemical kinetics of methane, and the availability of multidimensional numerical codes that can be used for micro-combustor design.

In this work, the catalytic and gas phase combustion in a methane-fueled micro-combustor with the supported noble metal catalyst Pt/γ-Al_2O_3 washcoat was investigated numerically. Numerical simulations with detailed gas phase and surface catalytic reaction mechanisms of methane-air mixtures are investigated by using the FLUENT 6.3.26 [16] coupled with the DETCHEM 2.4 [17]. The elementary catalytic and gas phase chemical reaction schemes were included along with external heat losses, surface radiation heat transfer, and heat conduction in the walls of the micro-chamber. The main theme of this study was to investigate the interaction of catalytic and gas phase combustion, transport and heat transfer mechanisms in the micro-combustor, and to delineate combustion stability limits according to the underlying parameters.

NUMERICAL MODELS AND SIMULATION APPROACH

Model geometry and mesh

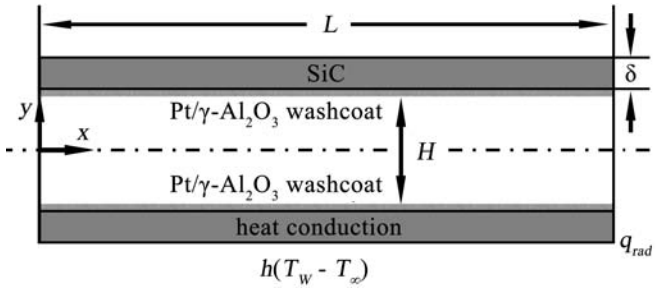

Figure 1. *Schematic diagram of the micro-combustor*

The geometry of the plane channel used in this study is presented in Fig. 1. The FLUENT 6.3.26 coupled with the DETCHEM 2.4 was used to simulate the flow in the plane channel of length L = 10.0 mm, height H =1.0 mm and wall thickness δ = 0.1 mm. Inner horizontal channel surfaces contained Pt/γ-Al_2O_3 catalyst washcoat. The site density (Γ) for this supported noble metal catalyst was taken as 2.7×10^{-9} mol·cm^{-2}. The properties of Pt/γ-Al_2O_3 catalyst washcoat are shown in Table 1.

Table 1. *The properties of Pt/γ-Al_2O_3 catalyst washcoat*

Property	Value
Catalyst surface site density Γ [mol·cm^{-2}]	2.7×10^{-9}
Average pore diameter d_{pore} [m]	2.08×10^{-8}
Catalyst porosity ε_{cat}	0.4
Catalyst tortuosity τ_{cat}	8.0

The incoming methane-air flow was fully premixed with an equivalence ratio (φ) of 0.4; it had uniform inlet pressures of 0.1 or 0.6 MPa (i.e. p = 0.1 or 0.6 MPa). In order to sustain micro-combustion of fuel-lean methane-air mixtures over Pt/γ-Al_2O_3 [18], the methane-air mixtures were preheated to 600 or 700 K (i.e. inlet temperature T_{in} = 600 or

700 K). The preheated methane-air mixtures can be accomplished with heat-recirculating or excess enthalpy micro-combustors in practice [2]. For all scenarios analyzed in this work, the uniform grid size of 5μm was used to mesh the 2-D models for the CFD simulations. This delicate mesh size provided a good spatial resolution for the most varied distributions in the micro-combustor.

Mathematical model and boundary conditions

In order to couple the fluid dynamics, heat transfer, and hetero-/homogeneous reaction of the methane-air mixtures, an external program DETCHEM 2.4 is used as UDF (user defined function) to FLUENT 6.3.26 to extend the modeling capabilities in simulating the detailed gas phase and surface catalytic chemical kinetics. The DETCHEM software package is designed for modeling and simulation of reactive flows, including heterogeneous reactions on catalysts and can apply multi-step and elementary chemical reaction mechanisms in the gas phase and on surfaces [17]. The CFD simulation convergence is judged upon the residuals of all governing equations. The governing equations for a steady, laminar, 2-D reactive flow with surface catalytic reactions are as follows:

Continuity equation:

$$\frac{\partial \rho}{\partial t}+\frac{\partial}{\partial x_j}(\rho u_j)=0 \tag{1}$$

Composition equation:

$$\rho\frac{\partial Y_s}{\partial t}+\rho u_j\frac{\partial Y_s}{\partial x_j}=\frac{\partial}{\partial x_j}\left(D\rho\frac{\partial Y_s}{\partial x_j}\right)+R_s \tag{2}$$

where R_s is the consumption or generation rate of species s. On the catalytic surface, R_s is given by

$$R_s M_s = -D\rho\left(\frac{\partial Y_s}{\partial n}\right)+Y_{s,w}\rho_w u_n \tag{3}$$

where M_s is the molar mass of species s. u_n is the velocity component of Stefan flow near and perpendicular to the wall. R_s is determined according to the following formula:

$$R_s=\sum_{k=1}^{K_s}\nu_{rs}k_r\prod_{j=1}^{N_g+N_s}[x_j]^{\nu'_{jr}}\left(i=1,\cdots,N_g+N_s\right) \tag{4}$$

where χ_j is the concentration of species j, which unit is mol·m^{-2} when it is adsorbed surface species. Ks are the number of surface elementary reactions. N_g+N_s are the number of species. ν_{rs} and ν'_{jr} are the stoichiometric coefficients. k_r is the reaction rate constant of the r reaction step, and determined according to the Arrhenius expression as follows:

$$kr=A_r T^{\beta r}exp\left(-\frac{E_{ar}}{RT}\right)\cdot\prod_{s=1}^{Ns}\Theta_s^{\mu_{rs}}exp\left(-\frac{\varepsilon_{rs}\Theta_s}{RT}\right) \tag{5}$$

where A_r, β_r, E_{ar}, R, T, and Θ_s are the pre-exponential factor, temperature exponent, activation energy, gas constant, temperature, and surface coverage in the Arrhenius expression. μ_{rs} and ε_{rs} are the coverage parameters.

Momentum equation:

$$\frac{\partial}{\partial t}(\rho u_i)+\frac{\partial}{\partial x_j}(\rho u_j u_i)=\frac{\partial p}{\partial xi}+\frac{\partial}{\partial x_j}\left[\mu\left(\frac{\partial u_i}{\partial x_j}+\frac{\partial u_j}{\partial x_i}\right)\right] \quad (6)$$

Energy equation:

$$\rho\frac{Dh}{Dt}-\frac{\partial P}{\partial t}=\frac{\partial}{\partial x_j}\left[\lambda\frac{\partial T}{\partial x_j}\right]+\frac{\partial}{\partial x_j}\left[\lambda\sum_s D_s\rho\frac{\partial Y_s}{\partial x_j}h_s\right]+q \quad (7)$$

where h and h_s are the enthalpy change and the enthalpy of the species s, which are given by

$$h=\sum Y_s h_s \quad (8)$$

$$h_s=\int c_p s dT+h_{0s} \quad (9)$$

q is the thermal effect of the reaction in Eq. (7). On the catalytic surface, q is given by

$$q=\sum_{s=N_g}^{N_g+N_s} H_s^{\,0} R_s M_s \quad (10)$$

where $H_s^{\,0}$ is the standard enthalpy of formation of species s.
The ideal gas law:

$$p=\rho RT\sum\frac{Y_s}{M_s} \quad (11)$$

The numerical simulation approach was adopted for the heat conduction in the wall of micro-chamber, and the solid thermal conductivity is k_s. The external heat losses were imposed at the outer wall surface of the micro-chamber, according to $h(T_w - T_\infty)$ with the heat transfer coefficient h, the outer wall surface temperature T_w, and the ambient temperature T_∞=298 K. The parametric studies of micro-combustor were carried out by varying the solid thermal conductivity k_s, the heat transfer coefficient h, and the inlet velocity V_{in}.
The radiation consists of the heat transfer exchange between the discretized catalytic surface elements as well as between each catalytic surface element and the inlet and outlet sections of micro-combustor, which was calculated by the net radiation method for gray and diffuse areas. The emissivity (inlet, outlet, and catalytic surface element) was all equal and the radiation exchange temperatures of the inlet and outlet sections were equal to the corresponding mean temperatures of the gas mixture. For the kth channel catalytic surface element, the radiation balance is given by

$$q_k=\varepsilon\sum_{j=1}^{N+2}F_{k-j}\sigma\left(T_k^4-T_j^4\right)+\sum_{j=1}^{N+2}(1-\varepsilon)F_{k-j}q_j \quad (12)$$

where q_k is the radiant flux, F_{k-j} is the configuration factor between the finite areas k and j, and j runs over the N channel catalytic surface elements as well as the inlet and outlet sections.
The emissivity of all surfaces (inlet, outlet, and catalytic surface) was constant at $\varepsilon = 0.5$ in the bulk of the ensuing computations. Due to the heavy nitrogen dilution and the micro-scale optical paths, the gas radiative emission and absorption in this study were not considered. The radiative boundary conditions of the solid phase were applied on the vertical wall surfaces of inlet and outlet sections.

Chemical kinetics

The detailed chemical kinetic mechanisms were used on the catalyst washcoat (Pt/γ-Al_2O_3) and in the gas phase of the micro-combustor. The elementary surface catalytic reaction mechanism shown in Table 2 (24 reaction steps, 11 surface species and 9 gaseous species) was used to describe the Surface reactions of methane on Pt/γ-Al_2O_3 washcoat, which was adopted from the mechanism presented by DETCHEM 2.4 [17, 19] (developed by the research group of Olaf Deutschmann, Karlsruhe Institute of Technology, Germany, 2013).

Table 2. *Surface catalytic reaction mechanism of methane on Pt/γ-Al_2O_3 washcoat* [a]

	Reaction	A	b	E_a/ (KJ·mol^{-1})	$\varepsilon_{rs}, \mu_{rs}$ [b]
(1)	$H_2 + 2Pt(S) \rightarrow 2H(S)$	4.60×10^{-2}	0.0	0.0	$\mu_{Pt(s)} = -1.0$ [c]
(2)	$2H(S) \rightarrow H_2 + 2Pt(S)$	3.70×10^{21}	0.0	67.4	$\varepsilon_{H(S)} = 6.0$
(3)	$H + Pt(S) \rightarrow H(S)$	1.00			[c]
(4)	$O_2 + 2Pt(S) \rightarrow 2O(S)$	1.80×10^{21}	-0.5	0.0	
(5)	$O_2 + 2Pt(S) \rightarrow 2O(S)$	2.30×10^{-2}			[c]
(6)	$2O(S) \rightarrow O_2 + 2Pt(S)$	3.70×10^{21}	0.0	213.2	$\varepsilon_{O(S)} = 60.0$
(7)	$O + Pt(S) \rightarrow O(S)$	1.00			[c]
(8)	$H_2O + Pt(S) \rightarrow H_2O(S)$	0.75			[c]
(9)	$H_2O(S) \rightarrow H_2O + Pt(S)$	1.00×10^{13}	0.0	40.3	
(10)	$OH + Pt(S) \rightarrow OH(S)$	1.00			[c]
(11)	$OH(S) \rightarrow OH + Pt(S)$	1.00×10^{13}	0.0	192.8	
(12)	$H(S) + O(S) = OH(S) + Pt(S)$	3.70×10^{21}	0.0	11.5	
(13)	$H(S) + OH(S) = H_2O(S) + Pt(S)$	3.70×10^{21}	0.0	17.4	
(14)	$OH(S) + OH(S) = H_2O(S) + O(S)$	3.70×10^{21}	0.0	48.2	
(15)	$CO + Pt(S) \rightarrow CO(S)$	8.40×10^{-1}			$\mu_{Pt(s)} = 1.0$ [c]
(16)	$CO (S) \rightarrow CO + Pt(S)$	1.00×10^{13}	0.0	125.5	
(17)	$CO_2(S) \rightarrow CO_2 + Pt(S)$	1.00×10^{13}	0.0	20.5	
(18)	$CO + O(S) \rightarrow CO_2(S) + Pt(S)$	3.70×10^{21}	0.0	105.0	
(19)	$CH_4 + 2Pt(S) \rightarrow CH_3(S) + H(S)$	1.00×10^{-2}			$\mu_{Pt(s)} = 0.3$ [c]
(20)	$CH_3(S) + Pt(S) \rightarrow CH_2(S) + H(S)$	3.70×10^{21}	0.0	20.0	
(21)	$CH_2(S) + Pt(S) \rightarrow CH(S) + H(S)$	3.70×10^{21}	0.0	20.0	
(22)	$CH(S) + Pt(S) \rightarrow C(S) + H(S)$	3.70×10^{21}	0.0	20.0	
(23)	$C(S) + O(S) \rightarrow CO(S) + Pt(S)$	3.70×10^{21}	0.0	62.8	
(24)	$CO(S) + Pt(S) \rightarrow C(S) + O(S)$	1.00×10^{18}	0.0	184.0	

[a] A: pre-exponential factor; b: temperature exponent; E_a: activation energy. Reactions (4) and (5) represent the alternative competing pathways.
[b] According to Eq. (5); [c] Sticking coefficient.

The elementary gas phase reaction mechanism was adopted from the mechanism presented by GRI-Mech 3.0 [20], which is a compilation of 325 elementary chemical reactions and associated rate coefficient expressions and thermochemical parameters for the 53 species involved in them. The conditions for which GRI-Mech 3.0 was optimized, limited primarily by availability of reliable optimization targets, are roughly 1000 to 2500 K, 1.3 KPa to 1.0 MPa, and equivalence ratio from 0.1 to 5 for premixed systems. Gaseous and surface thermodynamic data were included in the provided schemes (DETCHEM 2.4 and GRI-Mech 3.0).

The above-mentioned reaction mechanisms have been used in the previous studies [21-24] and the comparisons with experimental results were satisfactory. The gas phase multicomponent viscosities, thermal conductivities, diffusion coefficients, and thermal diffusion coefficients were adopted from the transport model presented by a TRANSPORT software package of CHEMKIN-PRO 15131 [25].
The numerical simulations were performed on 2.4GHz×4 Xeon 7440 processors with 32 GB of RAM each. When parallel processing was used, the message passing interface (MPI) was used to transmit information between nodes. The natural parameter continuation was implemented in order to achieve convergence as well as compute extinction points. The calculation time of each 2-D simulation varied between 2 and 8 hours, depending on the initial guess and the difficulty of the problem.

RESULTS AND DISCUSSION

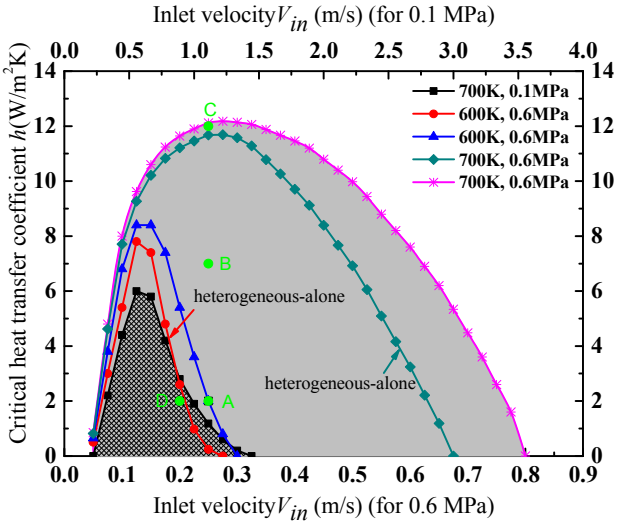

Figure 2. *The stability diagrams of micro-combustion in terms of the inlet velocity V_{in} and the critical heat transfer coefficient h. The fuel is methane and the equivalence ratio φ is 0.4. For the 700 K cases, the micro-combustion stable regimes of methane/air mixtures are shown by the shaded areas. Heterogeneous-alone reaction means pure catalytic reaction without gas phase reaction*

The stability diagrams of micro-combustion have been constructed by varying independently the solid wall thermal conductivity k_s, the external heat transfer coefficient h, and the inlet velocity V_{in}. Figure 2 presents the stability diagrams of micro-combustion. For this study, the solid wall thermal conductivity k_s and the emissivity ε are 2.0 W·m^{-1}·K^{-1} and 0.5, respectively. Therein, stability diagrams for T_{in} is 600 K (0.6 MPa) or 700 K (0.1 or 0.6 MPa) were simulated by one parameter continuation for the given V_{in} until the critical heat transfer coefficient h was reached. In this case, two different velocity scales are employed in Fig. 2 in order to facilitate the forthcoming comparison of the inlet pressures p = 0.1 or 0.6 MPa stability limits at the given mass flow rate. The stability limits at low inlet velocity V_{in} limits are derived from

extinction due to the heat loss, whereas at large inlet velocity V_{in} define blowouts due to the insufficient residence times.

Micro-combustion coupling of heat transfer and chemical kinetics

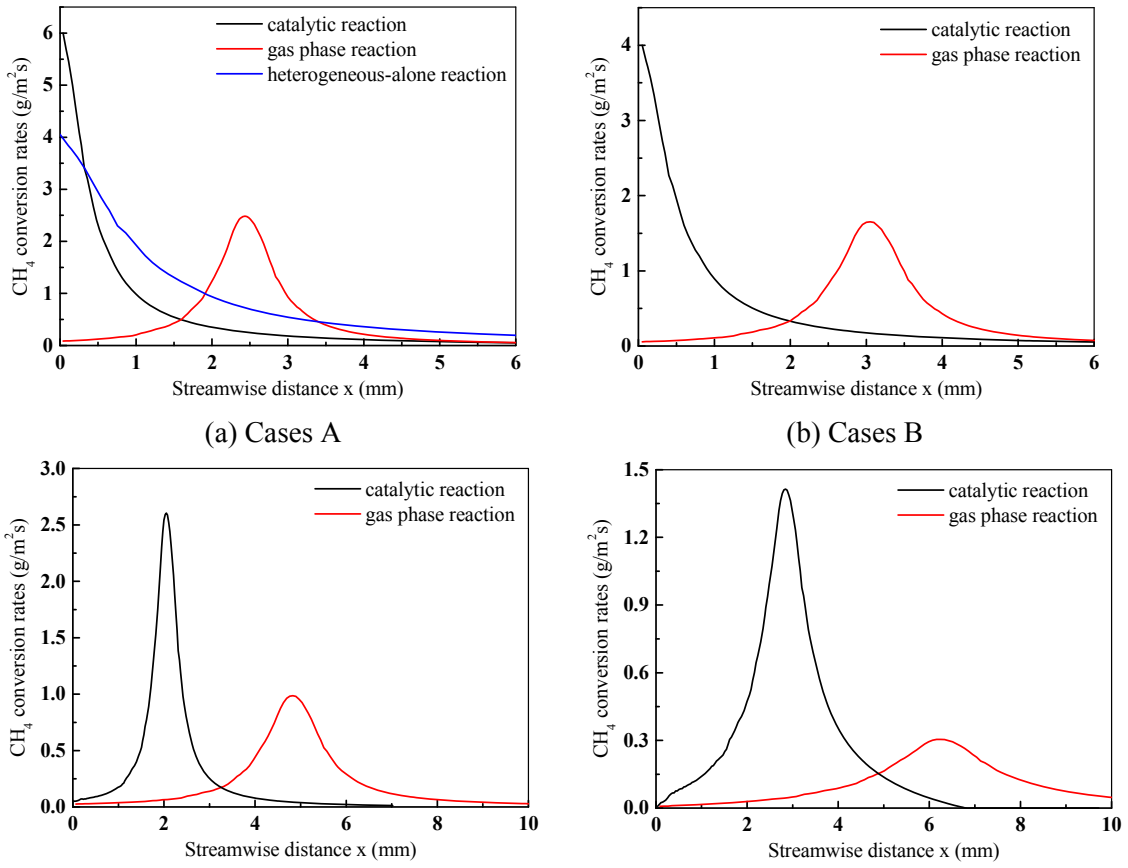

Figure 3. *CH_4 conversion rates of gas phase and catalytic reaction across the half-height of plane channel for the four designated cases in Fig. 2: Cases A, B, C (T_{in}: 700 K, p: 0.6 MPa, V_{in}: 0.25 m·s^{-1}) and Case D (T_{in}: 700 K, p: 0.1 MPa, V_{in}: 1.0 m·s^{-1})*

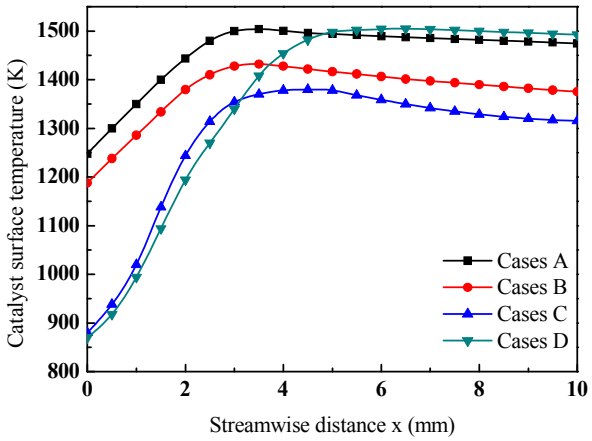

Figure 4. *Pt/γ-Al_2O_3 catalyst surface temperature profiles for the four designated cases in Fig. 2. : Cases A, B, C (T_{in}: 700 K, p: 0.6 MPa, V_{in}: 0.25 m·s^{-1}) and Case D (T_{in}: 700 K, p: 0.1 MPa, V_{in}: 1.0 m·s^{-1})*

In this case, four combinations of the critical heat transfer coefficient h and the inlet velocity V_{in} (indicated by points A, B, C, and D in Fig. 2) are applied. The inlet pressure and temperature of cases A-C are 0.6 MPa and 700 K, and Case D is 0.1 MPa and 700 K. The results shown in Fig. 3 indicate the streamwise profiles of the local gas phase and catalytic CH_4 conversion rates. In order to provide the CH_4 conversion rate per unit wall area of micro-combustor, the direct comparison results of surface catalytic and gas phase CH_4 conversion rates have been integrated across the half-height of plane channel in Figure 3. The corresponding surface temperatures of catalyst Pt/γ-Al_2O_3 are shown in Figure 4. Distributions of fuel (CH_4) and OH mass fractions, temperature, and gaseous heat release rate are shown in Figure 5.

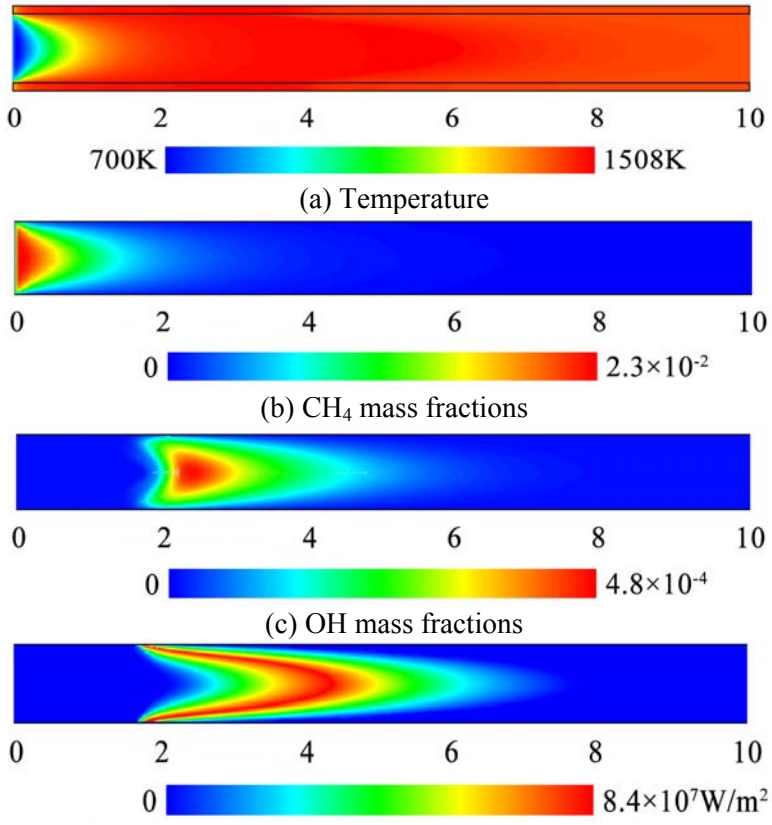

Figure 5. *Distributions of temperature, mass fractions (CH_4 and OH), and gaseous heat release rate for the Case A in Fig. 2*

For the case A (Figure 3a), there is the significant gas phase CH_4 conversion rates that lead to the formation of the strong combustion as illustrated in Figure 5. The flame of micro-combustion is anchored near the catalytic wall at streamwise distance x = 2.0 mm, which indicated by the profile of gaseous heat release rate in Figure 5d. Due to the catalytic depletion of CH_4 in the vicinity of the catalytic wall in Figure 5b, the most vigorous gaseous heat release rate occurs at the center of the plane channel farther downstream between 3.0 and 5.0 mm. The flame temperature of micro-combustion at the center of the plane channel is only 24 K higher than the catalytic local wall temperature all the same in Figure 5a. The complete conversion of CH_4 is attained at the

exit of micro-combustion for all Cases (Case A is shown in Figure 5b), and the hetero-/homogeneous reaction pathways compete for CH_4 consumption in the plane channel.
In most previous computational studies of micro-scale catalytic combustion, the gas phase reactions have been generally neglected. However, the gas phase reactions significantly effect on the micro-combustion characteristics under most of the conditions computational studied. When the flame is anchored in the micro-combustor, the spatial extent of CH_4 consumption and the heat release zones becomes narrower. The CH_4 catalytic conversion rates profile (shown in Figure 3a) is significantly longer when gas phase reactions are ignored. To external heat losses, the heat release of localized gas phase reactions is more resilient than the catalytic reactions, which are more broadly distributed of heat release. In terms of micro-combustion stability of the methane-air mixtures, the presence of gas phase reactions extends mildly the stability limits of micro-combustion at low and moderate inlet velocities (Figure 2). At higher inlet velocities of the methane-air mixtures, the catalytic reactions may not attain CH_4 accomplish conversion when the extinction limits of micro-combustion are approached, due to the effects of the finite rate catalytic reactions (Figure 2). In the higher inlet velocity cases, gas phase reactions have a more profound effect on extending the stability limits of micro-combustion by allowing for additional heat release in the plane channel. The above mentioned results are shown by two added heterogeneous-alone stability diagrams of micro-combustion in Figure 2 (T_{in}: 700 and 600 K, p: 0.6 MPa), which were simulated without gas phase reaction (i.e. pure catalytic reaction).
Micro-combustion stable regimes of methane-air mixtures narrow substantially at p: 0.6 MPa, T_{in}: 600 K, and φ: 0.4, particularly in terms of V_{in} (shown in Figure 2). Therefore, the sufficient preheat of the fuel/air mixtures is necessary for extended micro-combustion stability limits in fuel-lean combustion. For the T_{in}: 700K case, when the same mass flow rate ($\rho_{in} \times V_{in}$) is considered, the micro-combustion stability limits at p: 0.1 MPa are much narrower than at p: 0.6 MPa. The reason is that both the gas phase and catalytic reaction activities decline with decreasing pressure (i.e. decreasing concentration).

Effect of wall thermal conductivity

In terms of the critical heat transfer coefficient h for extinction, micro-combustion stability limits are provided in Fig. 6 for T_{in}: 700K, p: 0.6 MPa, and two inlet velocities V_{in}: 0.25 and 0.5 m/s. For low thermal conductivity materials, for example $k_s < 2.0$ $W \cdot m^{-1} \cdot K^{-1}$, the reduced upstream heat transfer from the post-combustion region hinders catalytic ignition and causes blowout. For higher inlet velocities V_{in}: 0.5 $m \cdot s^{-1}$, the micro-combustion stability limits at low thermal conductivity k_s are narrower. In comparison to homogeneous combustion (i.e. pure gas phase combustion) studies [18], there are marked differences at the low thermal conductivity k_s behavior, which is discussed qualitatively, since the aforementioned study refers to different operating conditions and model geometry. In homogeneous combustion, the micro-combustion blowout limits extend over the narrower range of the thermal conductivity k_s ($\approx$ 0.4-0.8 $W \cdot m^{-1} \cdot K^{-1}$) and are nearly independent of the critical heat transfer coefficient h (the blowout limit line of micro-combustion is almost parallel to the h-axis). The reason is low thermal conductivity k_s reduce the heat conduction away from the post-combustion region to upstream for preheating, and maintain moderate solid wall temperatures of

micro-combustor such that the external heat losses become less impact on removing heat from the solid walls. In addition, in the catalytic micro-combustor the distributed heat generation of the catalytic combustion provides the larger surface area with high solid wall temperatures, which lead to enhancing external heat losses in turn. Consequently, external heat losses play highly pivotal role in determining the micro-combustion stability limits of catalytic micro-combustor at low thermal conductivity k_s. Moreover, catalytic micro-combustor can achieve stable combustion compared to non-catalytic micro-combustor at low thermal conductivity k_s: the stable limits of micro-combustion extend to thermal conductivity $k_s < 0.1$ W·m^{-1}·K^{-1}, but there is little interest for such lower thermal conductivity materials in practice.

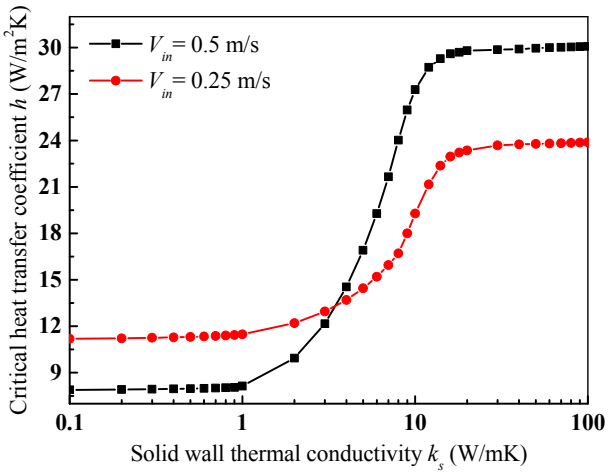

Figure 6. *Solid wall thermal conductivity k_s versus critical heat transfer coefficient h at different inlet mass velocities. The fuel is methane and the equivalence ratio φ is 0.4. The inlet temperature T_{in} and the inlet pressure p are 700 K and 0.6 MPa, respectively*

For the higher thermal conductivity k_s, the micro-combustion extinction limits reach their larger extent for thermal conductivity $k_s \approx 20.0$ W·m^{-1}·K^{-1}, and do not alter appreciably when thermal conductivity k_s is increased to 40.0 W·m^{-1}·K^{-1}. At low thermal conductivity k_s, the micro-combustion stability limits are defined by blowout and therefore the stability limits are narrower at higher inlet velocities V_{in}; whereas at large thermal conductivity k_s, the stability limits are heat-loss-induced and therefore the stability limits are wider at higher inlet velocities V_{in} in Fig. 6. In contrast, the pure gas phase combustion (i.e. homogeneous-alone combustion) exhibits the peak at thermal conductivity $k_s \approx 5.0$ W·m^{-1}·K^{-1}and further increase to thermal conductivity $k_s = 30.0$ W·m^{-1}·K^{-1}narrows down considerably the micro-combustion stable regimes [18, 26-28]. The reason is that the large thermal conductivity k_s result in efficient removal of the heat from the flame vicinity in pure gas phase combustion, and which eventually causes extinction in the micro-combustor. Despite the significant differences in the micro-combustion stability limits behavior of non-catalytic and catalytic micro-combustor, the maximum critical heat transfer coefficient $h \approx 30.0$ W·m^{-2}·K^{-1} in Fig. 6 is not quite different from which was reported in non-catalytic micro-combustor [18, 26-28].

Effect of surface radiation

In micro-combustor studies, the thermal radiation heat transfer from the high temperature catalytic surfaces is usually neglected. However, the thermal radiation can have a very strong effect not only on the micro-combustion stability limits, but also on the micro-combustion processes well-inside the stability region. The surface emissivity $\varepsilon = 0.5$ of catalytic micro-combustor was considered in the foregoing micro-combustion analysis. In Case A (p: 0.6 MPa and T_{in}: 700 K), which lies well-inside the micro-combustion stability diagram of Fig. 2, the surface temperatures of Pt/γ-Al_2O_3 catalyst are everywhere high and exceed 1240 K in Fig. 4. The detailed energy balance of the micro-combustor solid wall shows that the surface radiation is the mechanism of net heat loss over the entire catalytic surface length, the reason is that the heat is radiated towards the entry of significantly lower temperatures (inlet temperature $T_{\text{in}} = 700$ K). For different surface emissivities ε of Case A, the computed surface temperatures of Pt/γ-Al_2O_3 catalyst are shown in Figure 7. The simulation results of non-radiating (i.e. emissivity $\varepsilon = 0$) indicate substantially higher surface temperatures compared to the simulations results of emissivity $\varepsilon = 0.5$. The differences of simulation results are less pronounced, but still significant between the emissivity $\varepsilon = 0.5$ and 1.0 in Fig. 7. The above-mentioned simulation results are in qualitative agreement with simulation results of longer micro-scale catalytic monolithic channels (aspect ratio of 28) [29]: therein, increasing emissivity ε from 0 to unity caused the large temperatures drop at the entry of micro-combustor and also moved the peak solid wall temperatures farther downstream under the conditions where the light-off was accomplished practically at streamwise distance $x \approx 0$ mm (as in Fig. 3a and Figure 7). For the emissivity $\varepsilon > 0.5$ case, the Pt/γ-Al_2O_3 catalyst surface temperatures curves differed by less than 60 K in Figure 7 when the inlet and outlet sections of micro-combustor were treated as blackbodies (as in [29]).

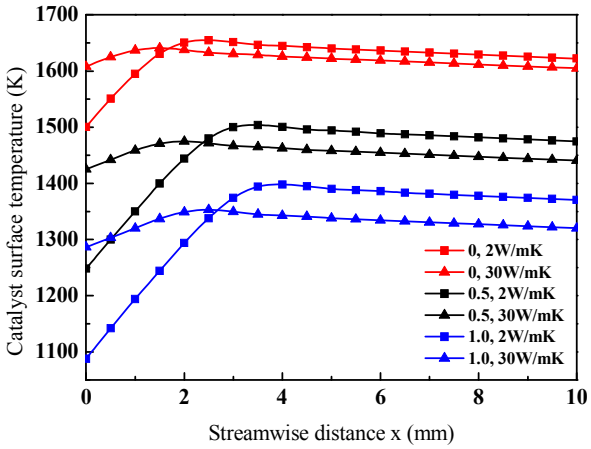

Figure 7. *Pt/γ-Al_2O_3 catalyst surface temperature profiles of Case A (T_{in}: 700 K, p: 0.6 MPa, V_{in}: 0.25 m·s^{-1}, h: 2.0 (W·m^{-2}·K^{-1}) for difference emissivities ε*

As the micro-combustion stability limits are approached, the role of radiation changes very drastically. For Case D (T_{in}: 700 K, p: 0.1 MPa, V_{in}: 1.0 m·s^{-1}, k_s: 2.0 (W·m^{-1}·K^{-1}), h: 2.0 W·m^{-2}·K^{-1}), the energy balance terms: net radiation Q_{rad}, convection to the gas Q_{conv}, integrated heat conduction Q_{cond}, Pt/γ-Al_2O_3 catalyst surface heat generation $Q_{\text{gen,cat}}$, and heat loss Q_{loss} across the solid wall thickness δ for each solid phase slice

(thickness δ and length Δx) of catalytic micro-combustor, that are shown in Figure 8. In order to facilitate the foregoing discussion, the gas phase heat generation $Q_{gen,gas}$ of the catalytic micro-combustor is not associated with the solid energy balance, which was included in Figure 8. Even though close to the micro-combustion stability limit for Case D, the heat loss Q_{loss} composes the small part of the entire solid energy balance although which is decisive. For Case D, the surface temperatures of Pt/γ-Al_2O_3 catalyst are low (less than 880 K in Case D of Figure 4) at the entry of catalytic micro-combustor such that the radiation heat losses are minimal for the front surface elements to the inlet sections (inlet temperature T_{in} = 700 K). This results in the positive net radiative heat flux Q_{rad} for the first 2.6 mm, and the negative net radiative heat flux Q_{rad} for the remaining length 2.6-10.0 mm in Figure 8; the heat is transferred from the post-combustion region (rear of the plane channel) to upstream (front of the plane channel) for preheating and that can improve the flame stability and thermal efficiency of micro-combustor. For Case D, numerical simulations with non-radiating surfaces (i.e. surface emissivity $\varepsilon = 0$) result in extinguishment of the micro-combustion, the reason is that the upstream radiation heat transfer in the plane channel was necessary for light-off of the catalytic micro-combustor. The same behavior (extinguishment) was also attested in Case C (T_{in}: 700 K, p: 0.6 MPa, V_{in}: 0.25 m·s^{-1}). However, the effect of radiation on reducing the entry temperatures of micro-combustor becomes less severe at larger thermal conductivity k_s (30.0 (W·m^{-1}·K^{-1}) in Figure 7.

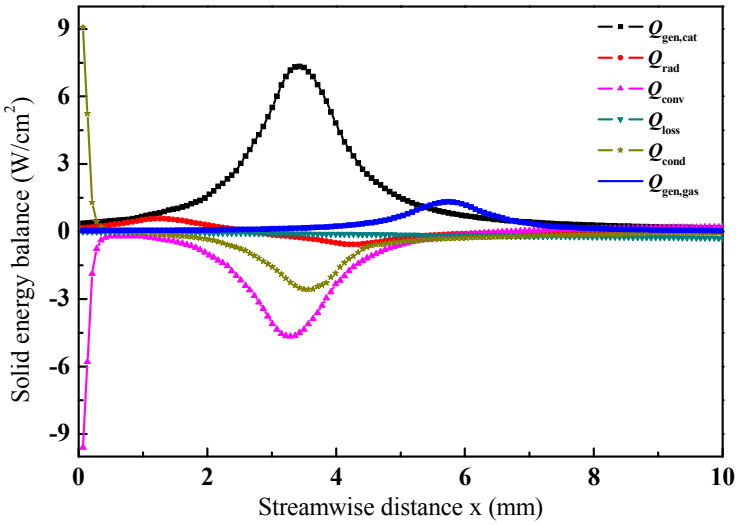

Figure 8. *The solid energy balance streamwise profiles of catalytic micro-combustor for Case D (T_{in}: 700 K, p: 0.1 MPa, V_{in}: 1.0 m·s^{-1}, k_s: 2.0 W·m^{-1}·K^{-1}, h: 2.0 W·m^{-2}·K^{-1})*

Effect of channel height

In this work, numerical simulations of micro-combustion characteristics were carried out for different channel heights (0.50 and 0.25 mm). The main objective was to assess whether the gas phase combustion of methane-air mixtures still plays a part in micro-scale catalytic combustion characteristics at such increased confinements. For Case A (T_{in}: 700 K, p: 0.6 MPa, V_{in}: 0.25 m·s^{-1}, k_s: 2.0 W·m^{-1}·K^{-1}, h: 2.0 W·m^{-2}·K^{-1}), Figure 9 shows the computed distributions of the OH mass fraction (Fig. 9 (a) and (c)) and the

gaseous heat release rate (Figure 9 (b) and (d)) for the two confinements of micro-combustion. At the sub-millimeter scale (0.50 and 0.25 mm), the gas phase combustion in catalytic micro-combustors can be sustained, and which intensity decreases with the decreasing channel height in Figure 9. Higher surface temperatures of Pt/γ-Al_2O_3 catalyst in the 0-2.0 mm of micro-combustors, which results in the flames move upstream with the decreasing channel height.

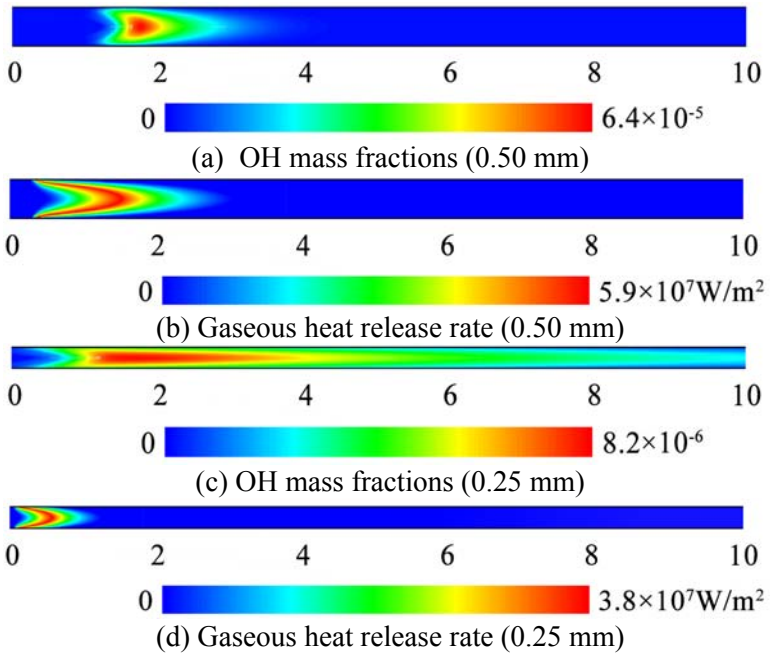

Figure 9. *Computed distributions of the OH mass fraction and the gaseous heat release rate for the two confinements (channel heights of 0.50 and 0.25 mm, respectively) of micro-combustion for Case A (T_{in}: 700 K, p: 0.6 MPa, V_{in}: 0.25 $m \cdot s^{-1}$, k_s: 2.0 $W \cdot m^{-1} \cdot K^{-1}$, h: 2.0 $W \cdot m^{-2} \cdot K^{-1}$). The fuel is methane and the equivalence ratio φ is 0.4*

CONCLUSIONS

In this study, micro-scale catalytic combustion characteristics and heat transfer processes of preheated methane-air mixtures (equivalence ratio φ of 0.4) in the plane channel were investigated numerically with detailed chemical kinetic mechanisms. The plane channel of length L = 10.0 mm, height H =1.0 mm and wall thickness δ = 0.1 mm, which inner horizontal surfaces contained Pt/γ-Al_2O_3 catalyst washcoat. The numerical model of micro-combustion was employed, which included heat transfer mechanisms and detailed gas phase and surface catalytic reaction mechanisms. The following conclusions were obtained from this micro-scale catalytic combustion characteristics study.

- The gas phase reactions significantly effect on the micro-scale catalytic combustion characteristics, and could not be ignored under most of the conditions computational studied.
- The presence of the gas phase reactions extends mildly the stability limits of micro-combustion at low and moderate inlet velocities of the methane-air mixtures. The gas phase reactions have a more profound effect on extending the stability limits of

micro-combustion by allowing for additional heat release in the plane channel at higher inlet velocities.

- When the same mass flow rate ($\rho_{in} \times V_{in}$) is considered, the micro-combustion stability limits at p: 0.1 MPa are much narrower than at p: 0.6 MPa due to both gas phase and catalytic reaction activities decline with decreasing pressure.
- Catalytic micro-combustor can achieve stable combustion compared to non-catalytic micro-combustor at low thermal conductivity k_s: the stable limits of micro-combustion extend to thermal conductivity $k_s < 0.1$ W·m^{-1}·K^{-1}.
- In homogeneous combustion, the micro-combustion blowout limits extend over the narrower range of the thermal conductivity k_s (≈ 0.4-0.8 W·m^{-1}·K^{-1}) and are nearly independent of the critical heat transfer coefficient h.
- The micro-combustion extinction limits reach their larger extent for the higher thermal conductivity k_s = 20.0-100.0 W·m^{-1}·K^{-1}.
- The micro-combustion stability limits of catalytic micro-combustors are wider than non-catalytic micro-combustors in comparison with the literature homogeneous-alone combustion (pure gas phase combustion) studies.
- The existence of the surface radiation heat transfer has two effects on the micro-scale catalytic combustion characteristics. The surface radiation moderates the solid wall temperatures, and is the net heat loss mechanism to the significantly lower temperatures entry over the entire catalytic surface length for the conditions far from extinction. However, the surface radiation near the stability borders can stabilize micro-scale catalytic combustion by redistributing the energy via heat transfer from the post-combustion region (rear of the plane channel) to upstream (front of the plane channel) for preheating and that can improve the flame stability, thermal efficiency, and light-off of catalytic micro-combustor.
- Finally, coupling with the exothermic surface catalytic reactions, the gas phase combustion in catalytic micro-combustors can be sustained at the sub-millimeter scale (plane channel height of 0.50 and 0.25 mm).

REFERENCES

1. Ju, Y., Maruta, K.: Microscale combustion: Technology development and fundamental research, *Progress in Energy and Combustion Science*, **2011, 37**, 669-715;
2. Maruta, K.: Micro and mesoscale combustion, *Proceedings of the Combustion Institute*, **2011, 33**, 125-150;
3. Walther, D. C., Ahn, J.: Advances and challenges in the development of power-generation systems at small scales, *Progress in Energy and Combustion Science*, **2011, 37**, 583-610;
4. Kaisare, N.S., Vlachos, D.G.: A review on microcombustion: Fundamentals, devices and applications, *Progress in Energy and Combustion Science*, **2012, 38**, 321-359;
5. Smyth, S.A., Kyritsis, D.C.: Experimental determination of the structure of catalytic micro-combustion flows over small-scale flat plates for methane and propane fuel, *Combustion and Flame*, **2012, 159**, 802-816;
6. Badra, J., Masri, A.R.: Design of a numerical microcombustor for diffusion flames, *Combustion Science and Technology*, **2012, 184**, 1121-1134;
7. Fanaee, S.A., Esfahani, J.A.: Two-dimensional analytical model of flame characteristic in catalytic micro-combustors for a hydrogen-air mixture, *International Journal of Hydrogen Energy*, **2014, 39**, 4600-4610;

8. Sadeghi, S.S., Tabejamaat, S., Baigmohammadi, M., Zarvandi, J.: An experimental study of the effects of equivalence ratio, mixture velocity and nitrogen dilution on methane/oxygen pre-mixed flame dynamics in a meso-scale reactor, *Energy Conversion and Management*, **2014, 81**, 169-183;
9. Sánchez-Sanz, M., Fernández-Galisteo, D., Kurdyumov, V.N.: Effect of the equivalence ratio, Damkohler number, Lewis number and heat release on the stability of laminar premixed flames in microchannels, *Combustion and Flame*, **2014, 161**, 1282-1293;
10. Bagheri, G., Hosseini, S.E., Wahid, M.A.: Effects of bluff body shape on the flame stability in premixed micro-combustion of hydrogen air mixture, *Applied Thermal Engineering*, **2014, 67**, 266-272;
11. An, H., Li, A., Sasmito, A.P., Kurnia, J.C., Jangam, S.V., Mujumdar, A.S.: Computational fluid dynamics (CFD) analysis of micro-reactor performance: Effect of various configurations, *Chemical Engineering Science*, **2012, 75**, 85-95;
12. Badra, J., Masri, A.R., Zhou, C.L., Haynes, B.S.: An experimental and numerical study of surface chemical interactions in the combustion of propylene over platinum, *Combustion and Flame*, **2013, 160**, 473-485;
13. Rana, U., Chakraborty, S., Som, S.K.: Thermodynamics of premixed combustion in a heat recirculating micro combustor, *Energy*, **2014, 68**, 510-518;
14. Li, Y.H., Chen, G.B., Wu, F.H., Cheng, T.S., Chao, Y.C.: Effects of catalyst segmentation with cavities on combustion enhancement of blended fuels in a micro channel, *Combustion and Flame*, **2012, 159**, 1644-1651;
15. Belmont, E.L., Ellzey, J.L.: Lean heptane and propane combustion in a non-catalytic parallel-plate counter-flow reactor, *Combustion and Flame*, **2014, 161**, 1055-1062;
16. Fluent 6.3 user's guide. Lebanon, New Hampshire: Fluent Inc., **2006**;
17. Deutschmann, O., Tischer, S., Kleditzsch, S., Janardhanan, V.M., Correa, C., Chatterjee, D., Mladenov, N., Mihn, H.D., Karadeniz, H.: DETCHEM Software package, 2.4 Ed., http://www.detchem.com, Karlsruhe, **2013**; accessed October **2014**;
18. Leach, T.T., Cadou, C.P., Jackson, G.S.: Effect of structural conduction and heat loss on combustion in micro-channels, *Combustion Theory and Modelling*, **2006, 10,** 85-103;
19. Deutschmann, O., Maier, L.I., Riedel, U., Stroemman, A.H., Dibble, R.W.: Hydrogen assisted catalytic combustion of methane on platinum, *Catalysis Today*, **2000, 59**, 141-150;
20. Smith, G.P., Golden, D.M., Frenklach, M., Moriarty, N.W., Eiteneer, B., Goldenberg, M., Bowman, C.T., Hanson, R.K., Song, S., Gardiner Jr., W.C., Lissianski, V.V., Qin, Z.W.: GRI-Mech 3.0, http://www.me.berkeley.edu/gri-mech/; accessed October **2014**;
21. Chan, D., Tischer, S., Heck, J., Diehm, C., Deutschmann, O.: Correlation between catalytic activity and catalytic surface area of a Pt/Al_2O_3 DOC: An experimental and microkinetic modeling study, *Applied Catalysis B: Environmental*, **2014, 156-157**, 153-165;
22. Shabanian, S.R., Rahimi, M., Khoshhal, A., Alsairafi, A.A.: CFD study on hydrogen-air premixed combustion in a micro scale chamber, *Iranian Journal of Chemistry & Chemical Engineering*, **2010, 29**, 161-172;
23. Leu, C.H., King, S.C., Chen, C.C., Huang, J.M., Tzeng, S.S., Liu, I.H., Chang, W.C.: Visible images of the catalytic combustion of methanol in a micro-channel reactor, *Chemical Engineering Journal*, **2013, 226**, 201-208;
24. Sadeghi, S.S., Tabejamaat, S., Baigmohammadi, M., Zarvandi, J.: An experimental study of the effects of equivalence ratio, mixture velocity and nitrogen dilution on methane/oxygen pre-mixed flame dynamics in a meso-scale reactor, *Energy Conversion and Management*, **2014, 81**, 169-183;
25. CHEMKIN-PRO 15131, Reaction Design: San Diego, **2013**;
26. Federici, J.A., Vlachos, D.G.: Experimental studies on syngas catalytic combustion on Pt/Al_2O_3 in a microreactor, *Combustion and Flame*, **2011. 158**, 2540-2543;
27. Federici, J.A., Wetzel, E.D., Geil, B.R., Vlachos, D.G.: Single channel and heat recirculation catalytic microburners: An experimental and computational fluid dynamics study, *Proceedings of the Combustion Institute*, **2009, 32**, 3011-3018;
28. Bijjula, K., Vlachos, D.G.: Catalytic ignition and autothermal combustion of JP-8 and its surrogates over a $Pt/\gamma\text{-}Al_2O_3$ catalyst, *Proceedings of the Combustion Institute*, **2011, 33**, 1801-1807;
29. Boehman, A.L.: Radiation heat transfer in catalytic monoliths, *AIChE Journal*, **1998, 44**, 2745-2755.